University of Groningen

Role of charge transfer configurations in LaMnO3, CaMnO3, and CaFeO3

Sadoc, Aymeric; Broer, Ria; de Graaf, Cornelis

IMPORTANT NOTE: You are advised to consult the publisher's version (publisher's PDF) if you wish to cite from it. Please check the document version below.

Document Version
Publisher's PDF, also known as Version of record

Link to publication in University of Groningen/UMCG research database

Role of charge transfer configurations in LaMnO$_3$, CaMnO$_3$, and CaFeO$_3$

Aymeric Sadoc and Ria Broer
Theoretical Chemistry, Zernike Institute for Advanced Materials, University of Groningen, Nijenborgh 4, 9747 AG Groningen, The Netherlands

Coen de Graaf
ICREA, Department of Physical and Inorganic Chemistry, Universitat Rovira i Virgili, Marcel·lí Domingo, s/n 43007 Tarragona, Spain

A simple scheme is proposed to analyze the *N*-electron wave function obtained in embedded cluster calculations in valence bond terms such as ligand-to-metal charge transfer and non-charge-transfer determinants. The analysis is based on a unitary transformation of pairs of natural orbitals to optimal atomiclike orbitals. The procedure is applied to compare the degree of ionicity in NiO and MnO and to explain the existence or absence of Jahn-Teller distortions in LaMnO$_3$, CaMnO$_3$, and CaFeO$_3$. The authors find that the ground state of LaMnO$_3$ is dominated by non-charge-transfer configurations, whereas the charge transfer configurations dominate the ground state wave function in the other two perovskites. © *2007 American Institute of Physics*. [DOI: 10.1063/1.2715552]

I. INTRODUCTION

The electronic structure of ionic transition metal compounds with strong electron correlation effects is intensively studied by solid-state scientists as well as quantum chemists. In solid-state physics and chemistry the electronic structure is most often described in terms of atom-centered orbitals, enabling an interpretation of the wave functions in valence bond (VB) terms, such as ionic and covalent structures and charge transfer (CT) between different sites. On the other hand, quantum chemistry commonly makes use of optimized orbitals, which normally have important contributions from different centers. Consequently, in quantum chemical approaches the importance of CT between different centers is not easily recognized in the *N*-electron wave function. This paper presents a simple procedure to translate the quantum chemical results in concepts often used in solid-state science.

As an example, we compare the degree of ionicity in NiO and MnO. Next, we investigate the importance of CT configurations for the presence or absence of distortions of the TMO$_6$ octahedra (TM=transition metal) found in LaMnO$_3$, CaMnO$_3$, and CaFeO$_3$. The first compound has strongly distorted octahedra with three different metal-oxygen distances. [1,2] CaMnO$_3$ and CaFeO$_3$ show important tilting effects of the octahedra, but the TM-O distances are equal. [3,4] The ionic model predicts LaMnO$_3$ as well as CaFeO$_3$ to have a transition metal $3d^4$ configuration and hence to be susceptible to Jahn-Teller distortions. The high formal charges of the metals in these three perovskites (Mn^{3+}, Mn^{4+}, and Fe^{4+}) put serious doubts on the applicability of the ionic model as starting point for the study of the electronic structure of these materials. The computational scheme applied in this study employs the embedded cluster approximation and provides a balanced, unbiased description of all important electronic configurations. We propose a simple scheme to analyze the *N*-electron wave function of the cluster in terms of non-charge-transfer and ligand-to-metal charge transfer contributions.

II. ELECTRON CORRELATION EFFECTS IN QUANTUM CHEMISTRY

The Hartree-Fock (HF) approach, in which the wave function consists of only one configuration state function (CSF), is not adequate for treating transition metal oxides due to the strong electron correlation effects in these materials. In quantum chemistry, the correlation energy is defined as the energy difference between the HF energy and the exact nonrelativistic energy. A distinction is often made between dynamical (mainly atomic) and nondynamical electron correlation effects. Dynamical correlation effects arise from the instantaneous electron-electron repulsion. Electrons avoid each other more effectively than predicted by the mean-field HF approach. Nondynamical (or molecular) correlation effects are caused by configurations that lie low in energy and strongly mix with the HF CSF.

A simple prototype example of the latter is the contribution of the $|\sigma_u^2|$ configuration in the wave function of a H$_2$ molecule. Around the equilibrium bond distance the HF wave function, which corresponds to the configuration $|\sigma_g^2|$, i.e., with both electrons in a bonding molecular $|\sigma_g|$ orbital, gives a reasonable approximation to the wave function. Alternatively, the HF wave function can be written in terms of localized atomlike orbitals l and r constituting σ_g: $\sigma_g \propto l + r$. The HF wave function contains equal contributions of covalent configurations $l^1 r^1$ and ionic configurations $l^2 + r^2$. When the molecule is stretched, this HF wave function is no longer a reasonable approximation: the contribution of the double bonding-to-antibonding excited $|\sigma_u^2|$ configuration must become stronger. Expressed in terms of l and r, the contribution of the ionic configurations $l^2 + r^2$ must become smaller.

The shortcomings of the HF wave function due to neglecting important nondynamical electron correlation effects are in some TM oxides already severe at the equilibrium bond distances. For a clear demonstration see, for example, the work on the MnO_4^- ion by Buijse and Baerends.[5] This very stable, nearly tetrahedral anion is in HF theory described as having five doubly occupied bonding orbitals. In tetrahedral symmetry three bonding orbitals transform according to t_2 and two transform according to e symmetry. Each of the five consists of a bonding combination of Mn-$3d$ and O-$2p$ atomic orbitals. Buijse and Baerends[5] showed that a reasonable wave function has to include at least bonding-to-antibonding excited configurations for each of these five bonding orbitals. Other studies that recognize the importance of this bonding-antibonding correlation can be found in Refs. 6–8.

In TM oxides with a sixfold, nearly octahedral oxygen coordination the bonding between transition metal and its coordinating ligands has a somewhat simpler appearance, because in octahedral geometry the TM-$3d$ t_{2g} orbitals interact only weakly with ligand orbital combinations of t_{2g} symmetry. The TM-ligand bonds are hence dominated by TM and ligand orbitals of e_g symmetry, which form bonding and antibonding combinations. Although an accurate treatment includes excitations from doubly occupied orbitals in both e_g and t_{2g} symmetries, neglecting excitations from t_{2g} orbitals is not as severe as for tetroxoanions such as MnO_4^-.

III. METHODS

The embedded cluster approximation is used to represent the materials. The crystal is divided into a cluster and an outer region. In the present study the clusters comprise one transition metal and its six oxygen neighbors. The ionic model is used to assign electrons to the ions present in the cluster. All cluster electrons are treated quantum mechanically, using the complete active space self-consistent-field (CASSCF) approximation outlined below. The outer region provides an appropriate representation for the rest of the crystal. The Coulomb and exchange interactions between the cluster electrons and those of the nearest ions in the crystal surrounding are represented by *ab initio* embedding model potentials (AIEMP's) centered at these nearest ions. These AIEMP's were introduced by Barandiarán and Seijo.[9] The electrostatic interactions of crystal ions further away from the cluster are represented by a large but limited set of point charges at lattice positions around the cluster. The value of the charges is optimized to accurately reproduce the Madelung potential (of the ionic crystal) on a fine grid in the whole cluster region.

A state-of-the-art quantum chemical scheme to account for electron correlation effects is the CASSCF method[10] in combination with the complete active space second-order perturbation theory (CASPT2) approach.[11,12] The most important part of the nondynamical correlation is accounted for by a CASSCF wave function that is constructed so as to include all relevant near-degenerate configurations; the remaining, mostly dynamical, electron correlation is estimated by the subsequent CASPT2.

Provided that a sufficiently large active space has been chosen, the CASSCF wave function accurately represents the charge distribution of a system. Accounting for the dynamical correlation has in many cases a major impact on the relative energies of the different N-electron states but leaves the general features of the N-electron wave function intact. Hence, the relative importance of charge transfer configurations can adequately be studied with extended CASSCF wave functions.

CASSCF divides the orbitals of the system in three different classes. The first contains the orbitals that are doubly occupied in all the CSFs. These orbitals are called the inactive orbitals and correspond typically to the core orbitals. The second class contains orbitals with occupation numbers between 0 and 2, the active orbitals. The number of electrons in the active space is defined by the total number of electrons minus two times the number of inactive orbitals. Under the usual spatial and spin symmetry restrictions, the wave function is written as a linear combination of all CSFs that can be formed by distributing the active electrons over the orbitals in the active space, i.e., a complete active space. Obviously, excitations from one orbital to another can only be included in the wave function if both orbitals are chosen in the active space. Finally, there is a set of orbitals that remain unoccupied in all electronic configurations of the CASSCF wave function, the so-called virtual orbitals. Although the virtual orbitals do not appear in the CASSCF wave function, they do play a very important role in the description of the dynamical electron correlation. CASSCF optimizes simultaneously the configuration expansion coefficients and the spatial shape of the orbitals.

The choice for a CAS expansion of the wave function implies the inclusion of highly excited configurations, which in general turn out to have negligible coefficients in the wave function expansion. The choice for a CAS expansion has, however, important advantages over a selected CSF expansion of the wave function. One advantage is that the orbital rotations among different active orbitals do not affect the energy of the system. This has important consequences for the analysis of the wave function as will be shown below.

Most commonly, the CASSCF wave function is expressed in a set of molecular orbitals that diagonalize the density matrix in the two sub-blocks (inactive and active molecular orbital spaces), the so-called natural orbitals. The eigenvalues correspond to the occupation numbers of these orbitals. This is, however, not the only possible choice to express the N-electron wave function. Natural orbitals are often delocalized over the whole system and this makes the interpretation in terms of VB configurations rather difficult. On the other hand, one can also opt to express the CASSCF wave function in terms of localized, atomiclike active orbitals, which enables the interpretation of the correlated wave function in VB structures. Combined with an ionic ansatz, this allows for an interpretation of the wave function in terms of non-charge-transfer (NCT), charge transfer (CT), double charge transfer (DCT),…, configurations, where NCT configurations agree with the ionic model.

The interpretation of accurate CASSCF wave functions in terms of VB structures has been the subject of extensive
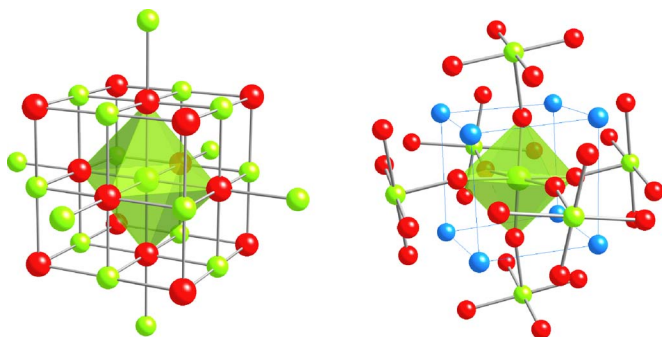
FIG. 1. (Color online) TMO_6 cluster in polyhedral view with $TM_{18}O_8$ AIEMP embedding for NiO and MnO (left), and $TM_6O_{24}A_8$ AIEMP embedding for $LaMnO_3$, $CaMnO_3$, and $CaFeO_3$ (right).

research. About a decade ago, Thorsteinsson et al.[13,14] examined transformations of CASSCF active orbitals to nonorthogonal VB orbitals. At about the same time, Hirao et al.[15] designed a CASVB method based on a transformation of the canonical CASSCF orbitals. The driving force for this earlier work was the same as ours, namely, to make contact with well-known chemical and physical concepts. An important difference is that the transformations in the present work consist of simple 2×2 rotations of selected pairs of active orbitals.

The transformations are determined as follows. First, two orbitals are selected in the active orbital space that transform according to the same symmetry species, where one orbital, ϕ_a, forms an antibonding combination between metal and ligands and the other, ϕ_b, forms the corresponding bonding orbital. It is usually possible to identify such bonding and antibonding orbital pairs when a suitable active orbital space has been chosen. Next two (symmetry-adapted) basis functions are selected that have non-negligible coefficients in both orbitals of the pair. In the present study, one basis function (χ_m) is centered on the metal and one (χ_l) on the ligands. Then, the ratios of the coefficients $c_{\chi_m}(\phi_b)/c_{\chi_l}(\phi_b)$ and $-c_{\chi_l}(\phi_a)/c_{\chi_m}(\phi_a)$ are considered as the arctangus of angles α_a and α_b. When the two orbitals can be viewed as a pair, the two angles are rather close. Next, the rotation angle α is determined as the average between α_a and α_b and the two orbitals are rotated,

$$
\begin{pmatrix} \cos \alpha & \sin \alpha \\ \sin \alpha & -\cos \alpha \end{pmatrix} \begin{pmatrix} \phi_a \\ \phi_b \end{pmatrix} = \begin{pmatrix} \phi_m \\ \phi_l \end{pmatrix},
$$

with ϕ_m the metal centered atomiclike orbital and ϕ_l the ligand centered one. Experience shows that the result is not very sensitive to the choice of basis functions χ_m and χ_l.

IV. COMPUTATIONAL INFORMATION

In the present study, we used the following systems: $[TMO_6]^{10-}TM_{18}O_8$ for NiO and MnO and $[TMO_6]^{x-}TM_6O_{24}A_8$ for $LaMnO_3$, $CaMnO_3$, and $CaFeO_3$, with $x=9$ for A=La and $x=8$ for A=Ca. A schematic view of the clusters used in the rocksalt oxides and perovskite materials is given in Fig. 1. The cluster is in brackets, and the other ions are represented by AIEMP's. The AIEMP's for all

systems except NiO were developed in the course of this study following the procedure described in Ref. 16. AIEMP's for NiO were taken from the MOLCAS basis set library.[17] The high formal cluster charge is stabilized by the Madelung potential represented by a set of optimized point charges.[18]

The basis set used to expand the one-electron orbitals is of atomic natural orbital type. A primitive set of $(21s, 15p, 10d, 6f)$ functions centered on the TM centers is contracted to a $(6s, 5p, 4d, 2f)$ basis set.[19] For the oxygen centered basis functions, we apply a $(14s, 9p, 4d)$ primitive set contracted to $(4s, 3p, 2d)$ basis functions.[20] In addition, we add $(1s, 1p)$ orthogonalization functions on the model potentials that represent TM ions in the cluster surrounding. These orthogonalization functions enable approximate strong orthogonality between cluster electrons and electrons represented by AIEMP's.[21] Details on the basis sets and the cluster embedding can be obtained from the authors.

For most of the calculations, the active space is formed by 12 orbitals and $4+n$ electrons. n is the number of d electrons associated with the TM in the ionic model. The number of active electrons varies between 12 for NiO (Ni^{2+}-$3d^8$) to 7 for $CaMnO_3$ (Mn^{4+}-$3d^3$). The 12 active orbitals include the mainly O-$2p$ orbitals of e_g character, formally doubly occupied in the ionic model, the five mainly TM-$3d$ orbitals, and five metal centered orbitals of the same symmetry character as the $3d$ orbitals with an extra radial node, the so-called $3d'$ orbitals.[22] An active space without TM-$3d'$ orbitals largely underestimates the importance of the charge transfer excitations, since these excitations can only become important when the wave function is flexible enough to account for the orbital relaxations that accompany charge transfer excitations in the configuration interaction (CI) expansion. Accounting for these relaxations requires at least the inclusion of ligand-$2p$ to TM-$3d$ replacements, coupled with single replacements to orbitals that are not occupied in the leading configuration.[23–26]

Although in O_h symmetry the TM-$3d$ t_{2g} orbitals interact only weakly with ligand orbital combinations of t_{2g} symmetry, the calculations on MnO, NiO, and $CaMnO_3$ were repeated with a larger active space, including not only the (mainly) O-$2p$ orbitals of e_g character but also those of t_{2g} character, in order to investigate the effect of excitations from mainly O-$2p$ orbitals of t_{2g} symmetry.

In the case of the perovskites, the orbitals were optimized for an average of states. For $LaMnO_3$ and $CaFeO_3$, we considered the two lowest quintet states corresponding to the two components of the ^5E_g (d^4) state of an undistorted octahedron. In the case of $CaMnO_3$, we considered an average of the $^4A_{2g}$ ground state and the first excited $^4T_{2g}$ state in the orbital optimization. This ensures that all five TM-$3d$ orbitals have an average natural occupation different from zero, avoids convergence problems associated with the correlating TM-$3d'$ orbitals, and allows us to use the same number of active orbitals in all the systems studied here. Root specific orbital optimization performed for $LaMnO_3$ gives virtually identical results.

TABLE I. Mulliken population analysis (in %) and occupation number n of the natural active orbitals in the ground state wave function of the embedded MnO_6 and NiO_6 clusters.

Orbital	MnO ($^6A_{1g}$)			NiO ($^3A_{2g}$)		
	n	Mn-$3d$	O-$2p$	n	Ni-$3d$	O-$2p$
$3e_g$	1.999	1.4	96.8	1.999	4.3	94.3
$2t_{2g}$	0.996	99.1	0.8	1.989	99.4	0.3
$4e_g$	0.996	97.0	3.3	0.997	94.0	5.8

All calculations performed for this study were done with the MOLCAS program suite developed in Lund by Karlström *et al.*[27] The orbital rotations were done with a program developed in the course of this study.

V. COVALENT INTERACTIONS: MnO VERSUS NiO

The ionic model, with TM^{2+} and O^{2-} ions, gives a useful first approximation to describe the binding between cations and anions in the late rocksalt-type transition metal oxides (TMO). It is commonly agreed that the covalent contributions to the TM-O bond increase with increasing nuclear charge. To illustrate the decrease in ionicity in going from MnO to NiO and to demonstrate our analysis, we compare the weight of CT configurations in the ground state of the TMO_6 clusters representing MnO and NiO. Using the optimal atomiclike orbital set obtained by our transformation, this weight gives a direct measure of the importance of the covalent interactions in these materials.

The ground state of the $[NiO_6]^{10-}$ cluster transforms following the A_{2g} irreducible representation of the O_h symmetry group and the ionic model predicts a spin-triplet coupled $[core3e_g^4 2t_{2g}^6 4e_g^2]$ electronic configuration. The CASSCF wave function is indeed dominated by this configuration. The character of the self-consistent active orbitals is listed in Table I. All other orbitals are less relevant to the binding between the TM and O. The ground state of MnO transforms as A_{1g} and is described by the spin-sextuplet coupled $[core3e_g^4 2t_{2g}^3 4e_g^2]$ electronic configuration in the simple ionic assumption. These orbitals are also analyzed in Table I.

The $3e_g$ natural orbitals are easily identified as O-$2p$ orbitals with small bonding tails on the TM, while the $4e_g$ orbitals form their antibonding counterpart, mainly localized on the TM. Compared to a CASSCF calculation with the $3e_g$ orbitals in the doubly occupied inactive space, the total energy is only slightly decreased, by 0.2 eV for NiO and 0.01 eV for MnO. Table I shows that the $2t_{2g}$ orbitals are almost pure TM orbitals, they have very weak antibonding contributions from the linear combination of O-$2p(t_{2g})$ orbitals. The contribution to the active orbitals of other types of basis functions, such as O-$2s$, is small in all cases.

Apart from the mixing of the O-$2p$ and TM-$3d$ basis functions in the orbitals, as shown in Table I, covalency can in principle also show up in the expansion of the N-electron wave function in CSFs. The complete active space of 9 electrons in 12 orbitals [CAS(9,12)] for the $^6A_{1g}$ state in MnO_6 gives rise to 11 646 CSFs. The CAS(12,12) for the $^3A_{2g}$ state in $[NiO_6]^{10-}$ leads to 95 391 CSFs. The leading $core3e_g^4 2t_{2g}^6 4e_g^2$ electronic configuration is characterized by

the occupation with four electrons of the O-$2p$ active orbitals. Besides configurations with four electrons of the mainly O-$2p$ active orbitals, which we denote NCT configurations following common practice, the CASSCF wave function expansion also contains CSFs with one or more (up to four) holes in the mainly O-$2p$ active orbitals. These configurations are usually labeled charge transfer (CT, one ligand hole), double CT (DCT, two ligand holes), triplet CT (TCT), and quadruple CT (QCT) configurations. Summing up all contributions of the different classes of CSFs, we observe that the NCT configurations are highly dominating in both wave functions. Their weights (squared coefficients) sum up to 99.9% in MnO and 99.6% in NiO. The CT configurations have a total weight of 0.1% in NiO and even less in MnO.

This analysis could lead to the conclusion that CT configurations are unimportant in both compounds and that only a weak covalency via the orbitals is observed, probably somewhat more pronounced in NiO than in MnO. However, the unitary transformation of the natural active orbitals to a set of atomiclike orbitals changes quite dramatically this first, intuitive impression. Figure 2 compares the original natural $3e_g$ and $4e_g$ orbitals of NiO_6 to the new optimal atomiclike orbitals. These transformed orbitals can be considered as the optimal choice of atomiclike orbitals to de-
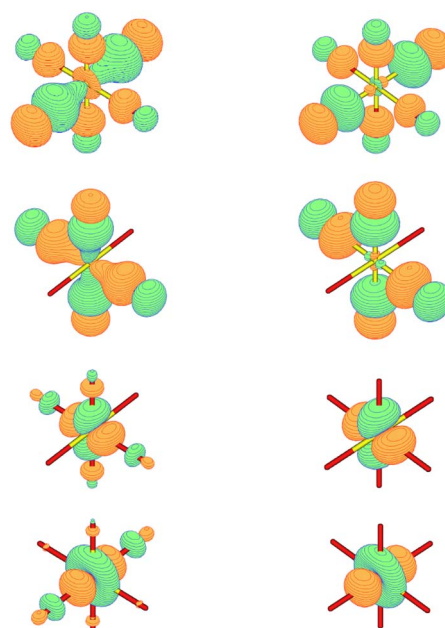

FIG. 2. (Color online) The $3e_g$ and $4e_g$ natural active orbitals (left) and the optimal atomic-like orbitals (right) for the $^3A_{2g}$ state of the embedded NiO_6 cluster.

scribe the bonding in the system under study. Optimal, because they are determined by a unitary transformation of optimized CASSCF orbitals. The transformation does not change the total energy of the system. It does, however, affect the coefficients of the different CSFs in the wave function. The covalency that showed up in the natural orbitals is now transferred to the wave function expansion, which makes the interpretation of the electronic structure easier. The Mulliken population analysis of the transformed orbitals gives the same results for NiO and MnO: in both cases the $4e_g$ orbitals have a weight of 100.6% on the TM and -0.5% on the oxygen ligand. For the $3e_g$ orbitals the numbers are inverted. Schematically denoted, the expansions of the wave functions are now

$$\Psi(MnO_6, {}^6A_{1g}):91.8\ \% \ \ NCT + 7.9\ \% \ \ CT + 0.1\ \%$$
$$DCT + \cdots ,$$

$$\Psi(NiO_6, {}^3A_{2g}):84.1\ \% \ \ NCT + 13.3\ \% \ \ CT + 0.3\ \%$$
$$DCT + \cdots .$$

The difference with the CI expansion in natural orbitals is striking. The weight of the NCT in the ${}^3A_{2g}$ wave function is lowered and the CT configurations increase their weight significantly. We can now even appreciate a (tiny) contribution of DCT configurations in the wave function. It is obvious from this analysis of the CASSCF wave function in optimal atomiclike orbitals that the covalent interactions in NiO are more important than in MnO. One may argue that allowing for excitations from O-$2p$ to Mn-$3d$ orbitals of t_{2g} symmetry might be important for MnO. Including a set of mainly O-$2p$ orbitals of t_{2g} symmetry in the active space leads, however, to a minor energy decrease of 0.04 eV. In NiO, where such excitations do not occur because the $2t_{2g}$ orbitals are (practically) doubly occupied, the energy decrease is negligible. There are now two sets of orbital pairs to transform, one set in t_{2g} symmetry and one in e_g symmetry. The weights of the NCT configuration become 87.8% for MnO and 82.7% for NiO.

The importance of orbital optimization becomes clear when the present results for NiO are contrasted to the relative weights of the NCT and CT configurations when the wave function is expressed in nonoptimized atomic orbitals. Such orbitals can be obtained, for example, by superimposing the charge distributions of a Ni^{2+} ion and a closed shell O_6^{12-} fragment, both embedded in point charges at the lattice positions of NiO. The ground state wave function of the NiO_6 cluster expressed in this nonoptimized atomic orbitals is

$$\Psi(NiO_6, {}^3A_{2g}):95.6\ \% \ \ NCT + 4.1\ \% \ \ CT + \cdots .$$

The decrease of the contribution of CT configurations is obvious, almost 10% less than for the optimal atomiclike orbitals.

Finally, we compare our results to those obtained by Casanovas et al.,[28] who estimated the covalent contributions to the wave function for NiO based on similar considerations as in this work. They performed large CI calculations using a set of nonoptimized atomic orbitals. The weight of the leading NCT configuration expressed in these orbitals is 81.7%

in the final CI wave function. The remaining $\approx 20\%$ can, however, not only be attributed to CT or DCT configurations, since the CI expansion of Casanovas et al. also contains many configurations that account for the optimization of the atomic orbitals. An advantage of our strategy is that the use of optimized atomic orbitals does not lead to extra configurations in the CI expansion of the wave function. This makes the analysis in terms of valence bond terms easier.

VI. JAHN-TELLER DISTORTIONS IN LaMnO₃, CaMnO₃, AND CaFeO₃

The observation of phenomena as the superconductivity in cuprates and ruthenates, colossal magnetoresistance in manganites, and charge ordering in many different perovskites, placed the transition metal perovskites at the center of present investigations in condensed matter physics. The coupling of the electronic structure to lattice deformations is an essential ingredient in the theoretical description of these phenomena.[29] Lattice deformations can either be dynamical in the form of polarons or static in the form of collective Jahn-Teller-type distortions. The description of Jahn-Teller distortions around impurities in ionic solids with embedded cluster models has shown to be very versatile, leading to a detailed understanding of the interplay between the electronic structure and the deformations around the impurity.[30,31] Here, we approach the problem of Jahn-Teller distortions in three different perovskites from a local point of view. The central question is whether the appearance or absence of static distortions can be understood with the analysis of the wave function in terms of optimal atomiclike orbitals as presented in the previous section.

For the simple cubic oxides treated in the previous section, the ionic model gives a reasonable starting point for the interpretation of the electronic structure. Nevertheless, important additional contributions appear in the wave function even for MnO, which has been considered as a prototype ionic material in many cases. In NiO and MnO the deviations from the ionic model can be caught quite well in the form of small orbital changes that occur in the CASSCF orbital optimization. Even with a small active space of five TM-$3d$ orbitals, a reasonable representation of the charge distribution is obtained. Increase of the active space with the five $3d'$ correlating orbitals and the occupied O-$2p$ e_g orbitals does not change the electron distribution significantly, because CT configurations are not very important. On the other hand, the validity of the ionic model as starting point for the three

TABLE II. Formal charge and number of TM-d electrons in the three perovskites considered. The prediction based on the ionic model for the local geometry around the TM is also given and compared to experimental findings.

	Charge	TM-$3d^x$	Ionic model	Expt.
LaMnO₃	3+	4	JT distortion	JT distortion[a]
CaMnO₃	4+	3	Octahedral	Octahedral[b]
CaFeO₃	4+	4	JT distortion	Octahedral 1[c]

[a]Reference 1.
[b]Reference 4.
[c]Results are compared to the high temperature phase of CaFeO₃ (Ref. 3).

TABLE III. Schematic representation of the wave function expansion expressed in natural and optimal atomiclike orbitals for $LaMnO_3$, $CaMnO_3$, and $CaFeO_3$. The weights of the different contributions are given in %.

Material	MO set	NCT	CT	DCT
$LaMnO_3$	Natural	98.0	0.9	0.3
	Atomic	58.0	38.8	3.2
$CaMnO_3$	Natural	96.3	2.0	2.6
	Atomic	20.9	55.9	20.4
$CaFeO_3$	Natural	85.5	7.2	4.6
	Atomic	18.1	66.1	13.6

distorted perovskite structures considered here is doubtful, because the model predicts high formal charges on the TM sites (Table II). These charges constitute a large attractive potential for the electrons associated with the O^{2-} ligands and CT or screening effects are expected to be quite important.

A. LaMnO₃

One-electron band structure calculations on the undoped compound $LaMnO_3$ show that the top of the valence band is a strong mixture of Mn-3d and O-2p states.[32–34] Although the top of the valence band can, of course, not directly be compared to the lowest N-electron state of an embedded cluster representing $LaMnO_3$, it is to be expected that the cluster calculation reflects this mixing by important covalent contributions to the wave function. Similar to the observations made for MnO and NiO, we find that the ground state CASSCF wave function has practically all its covalent interactions concentrated in the molecular orbitals. Firstly, there is one type of CSF that dominates the CI expansion, see the first row of Table III. Secondly, the Mulliken populations of the active orbitals indeed show some degree of mixing between the 2p basis functions centered at the oxygens and the Mn-3d basis functions (see Table IV). The t_{2g}-like active orbitals (19, 20, and 21a_g) are all occupied with one electron and highly localized on the Mn ion. For $LaMnO_3$ they are not further considered in the analysis of the electronic structure, but we will discuss excitations amongst orbitals of t_{2g} symmetry in some detail for $CaMnO_3$.

The leading determinant of the CASSCF wave function expressed in natural orbitals is $|core17a_g^2 18a_g^2 19a_g^1 20a_g^1 21a_g^1 22a_g^1 23a_g^0|$. Following the character of the orbitals given in Table IV, this leading determi-

nant corresponds (approximately) to the Mn-3d^4 (or NCT) configuration. The Mn-3d^4 ion in a weak octahedral crystal field has ^5E_g symmetry and is hence Jahn-Teller active. The dominant character of the NCT configuration is in agreement with the large distortion experimentally found in $LaMnO_3$. On the other hand, the present representation of the electron distribution does not clearly reflect the strong mixture of O-2p and Mn-3d found in the one-electron valence band. A more transparent analysis of the charge distribution can be made after the transformation to optimal atomiclike orbitals. The covalent interactions disappear from the orbitals and are transferred to the CI expansion of the wave function. Consequently, the weight of the NCT configuration with four Mn-3d electrons is strongly reduced, although it remains dominant, which makes the appearance of Jahn-Teller distortions in $LaMnO_3$ not unlikely. The importance of CT interactions is evident. The sum of all possible CT configurations gives 38.8%. Even DCT configurations show up with significant weights in the wave function.

The number of Mn-3d electrons, and consequently the total Mn charge, is also easily extracted from the wave function expressed in atomic orbitals. Given that the singly occupied t_{2g}-like natural active orbitals (19, 20, and 21a_g) can be considered to be atomiclike orbitals without significant O-2p contributions, the number of Mn-3d electrons x is given by $\Sigma_i \alpha_i x_i$. The sum runs over all the different configurations, and α_i and x_i correspond to the weights and the number of d electrons of these configurations. For $LaMnO_3$ this results in $x = 0.580 \times 4 + 0.388 \times 5 + 0.032 \times 6 = 4.45$. Since the Mn core has 18 electrons, the total charge at Mn is estimated to be +2.55.

B. CaMnO₃

The formal charge of Mn in $CaMnO_3$ is 4+, leading to a Mn-3d^3 $^4A_{2g}$ ground state. The higher formal Mn charge compared to $LaMnO_3$ makes it not unexpected that the contribution of covalent interactions to the Mn–O bond increases with respect to the the previous compound. The natural orbitals show a rather large mixing, the orbitals 17 and 18a_g now have 30% contribution from the Mn-3d centered basis functions. There is also a stronger mixing in the 22 and 23a_g orbitals, but this is less relevant since these orbitals are practically empty in the ground state. The transformation to atomic orbitals has dramatic consequences for the interpretation of the wave function. The weight of the NCT configuration is only 20% and CT configurations dominate the wave function. Furthermore, we observe that the DCT configura-

TABLE IV. Mulliken population analysis (in %) and occupation number n of the natural e_g-like active orbitals in the ground state wave functions of the embedded TMO_6 clusters representing $LaMnO_3$, $CaMnO_3$, and $CaFeO_3$.

Orbital	$LaMnO_3$			$CaMnO_3$			$CaFeO_3$		
	n	Mn-3d	O-2p	n	Mn-3d	O-2p	n	Fe-3d	O-2p
17a_g	1.996	9.0	92.2	1.945	30.3	72.0	1.983	33.3	70.1
18a_g	1.971	15.6	87.8	1.944	30.2	72.2	1.850	33.3	70.1
22a_g	1.000	86.0	13.8	0.005	73.1	26.2	1.012	67.1	33.1
23a_g	0.029	89.9	9.8	0.055	73.0	26.2	0.150	67.1	33.1

tions are as important as the NCT configurations. The calculated number of Mn-3d electrons is far away from the formal d^3 situation predicted by the ionic model. The dominance of the CT configurations leads to 3.88 d electrons and an effective charge of +3.12 for Mn in CaMnO$_3$.

The high formal charge of Mn in CaMnO$_3$ may give rise to CT not only from O-2p e_g orbitals but also to CT from O-2p orbitals of t_{2g} symmetry. Although the Mn-3d–O-2p interaction is much smaller, the active 2t_{2g} orbitals are essentially nonbonding 3d orbitals and the inactive 1t_{2g} orbitals are essentially O-2p orbitals that are nonbonding (with respect to Mn–O bonding), some effect of O-2p to Mn-3d excitations within t_{2g} symmetry may be expected.[5] To investigate this, we repeated the CASSCF calculations with a larger active space that also includes the 1t_{2g} orbitals. The effect on the total energy is, contrary to MnO, significant: the energy lowering is 1.7 eV. The weight of the NCT configurations decreases, to 17.1%, whereas that of DCT increases to 25.7%. The weight of single CT configurations is 53.5%, of which 46.3% is associated with transfer from e_g and 7.3% is associated with transfer from t_{2g} orbitals to Mn-3d.

Having established that Mn in CaMnO$_3$ is closer to a Mn-3d^4 ion than to the ionic assumption of Mn-3d^3, the question should be answered why this ion is not Jahn-Teller active, or in other words, why the ground state has A_{2g} symmetry and not E_g as for other d^4 systems. The key to the answer lies in the interaction between the NCT and CT configurations. In O_h terminology and expressed in atomic orbitals, the lowest CT CSF's are characterized by the [O-2p (e_g^3) Mn-3d (e_g^1) Mn-3d (t_{2g}^3)] electronic configuration, coupled to $E_g \otimes E_g \otimes A_{2g} = A_{1g}$, A_{2g}, E_g spatial symmetries. It is, however, only the $^4A_{2g}$ CSF that interacts with the lowest NCT CSF, which has also $^4A_{2g}$ symmetry. This interaction makes the $^4A_{2g}$ state the lowest N-electron state in the cluster. This ground state, although dominated by a Mn-3d^4L^{-1} configuration, is not Jahn-Teller active in agreement with experiment.

C. CaFeO$_3$

The ground state of a TM-3d^4 ion in a not too strong octahedral ligand field is ^5E_g. The tilting and rotation of the FeO$_6$ units in the high temperature phase of CaFeO$_3$ reduce the Fe site symmetry to C_i. The distortions of the Fe–O distances are, however, so small that the lowest two quintet states of the cluster ($a,b\ ^5A_g$) are still almost degenerate. The CASSCF energies of the two states differ by less than 0.05 eV, and the inclusion of dynamical electron correlation effects does not increase the splitting between the two quintet states.

The analysis of the wave function gives a rather similar picture as for CaMnO$_3$. The natural orbitals are 30/70 mixtures of O and Fe, and the CI expansion of the wave function in these orbitals is strongly dominated by the configurations with doubly occupied 17 and 18a_g orbitals. Because of the dominant oxygen character orbitals, these configurations could be labeled as NCT, but this leads to an incorrect picture of the electronic structure. The wave function expressed in optimal atomic orbitals is dominated by the CT
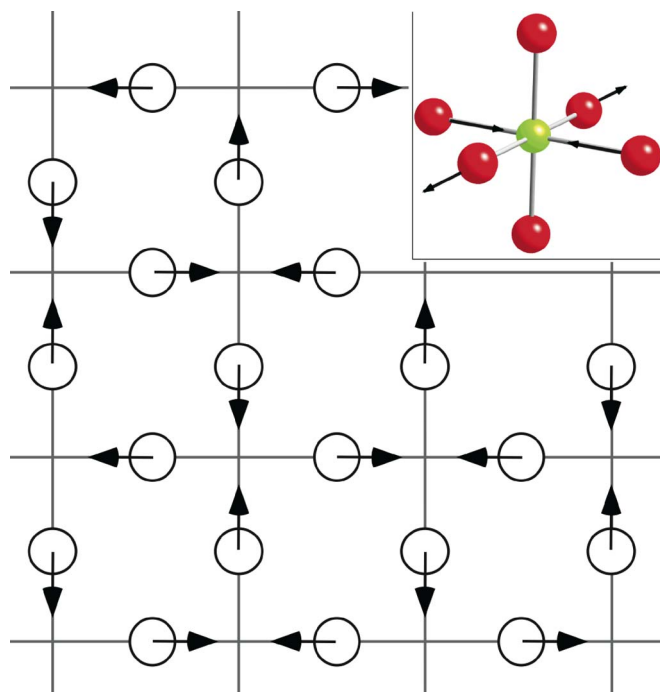

FIG. 3. (Color online) Oxygen displacements in the ab plane as observed in LaMnO$_3$. Mn ions (not shown) are situated at the crossing points of the gray lines. This collective distortion leads to two short and two long TM-O distances in the ab plane. The TM-O distance along the c axis is not affected. The inset shows the oxygen displacements in the TMO$_6$ cluster considered in the computational experiment.

(Fe-3d^5L^{-1}) configuration and has smaller contributions from the NCT and DCT configurations, see Table III. The dominant CT CSF's, 49% of the total wave function, are characterized as O-2p (e_g^3) Fe-3d ($t_{2g}^3e_g^2$) with the five Fe-3d electrons coupled to $^6A_{1g}$.

The calculated number of Fe-3d electrons is 4.85, which corresponds to a total charge of +3.16. Consequently, the iron ions in the high temperature phase of CaFeO$_3$ are best described as Fe^{3+} with five high spin coupled d electrons. These ions are not Jahn-Teller (JT) active. We should, however, also account for the possible distortions due to the hole in the oxygen orbitals. In the leading configurations of the ground state wave function, there are three electrons in 17 and 18a_g orbitals, which are e_g-like linear combinations of O-2p basis functions. Such electronic configurations can in principle be Jahn-Teller active. Recently García-Lastra *et al.* presented an appealing way to interpret Jahn-Teller distortions in terms of forces acting on the ligands by the charge distribution on the central ion.[35] Applying this concept to the present case, it is easily seen that the hole on the oxygens bridging two Fe-3d^5 ions exerts a symmetric force and no Jahn-Teller distortion is expected.

D. Cluster energy versus Jahn-Teller distortion

To further explore the possibilities of the cluster model approach to predict Jahn-Teller distortions in perovskites, we performed a computational experiment. Starting from clusters with equal TM-O distances in the ab plane, we gradually switch on the Jahn-Teller distortion by moving two oxygens inward and two oxygens outward (see Fig. 3). The TM-O
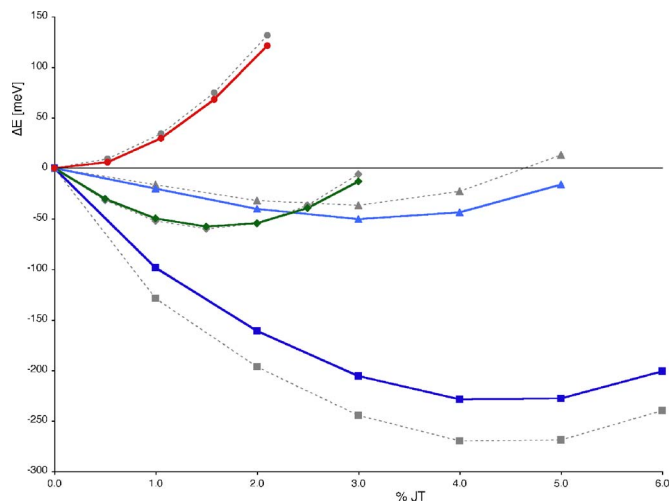
FIG. 4. (Color online) Relative CASPT2 energy of the ground state wave function as function of the distortion in embedded TMO_6 cluster representing LaMnO$_3$ (dark blue squares and light blue triangles), CaMnO$_3$ (red circles), and CaFeO$_3$ (green diamonds). The lines are a guide to the eyes. The dotted gray lines represent the CASSCF relative energies.

distance in the *c* direction is maintained at the experimental value and the initial TM-O distances in the *ab* plane are taken as the average of the corresponding experimental distances. This distortion mimics the collective movement of the oxygens in the *ab* plane observed in LaMnO$_3$. Figure 4 depicts the results of this series of calculations. The total CASPT2 energy in the undistorted cluster is taken as zero of energy and the index on the *x* axis is defined as the difference of the long and short TM-O bonds divided by the sum of them. We opt here for CASPT2 calculations in order to obtain as accurate as possible relative energies.

The continuous increase of the energy with the Jahn-Teller distortion for CaMnO$_3$ (red circles) confirms the tendency toward a perfect octahedral oxygen coordination of Mn in this compound. The situation is quite different for LaMnO$_3$. We first discuss the curve with the blue squares, which corresponds to a MnO$_6$ cluster embedded in model potentials and point charges at the experimental lattice positions. The cluster energy is strongly reduced by applying the Jahn-Teller distortion, and a minimum is observed at approximately 4.5%. The long and short Mn–O distances of 2.13 and 1.95 Å are not more than 0.05 Å shorter than the experimental distances. One could argue that the distortion is induced by the embedding crystal, which is based on the experimental LaMnO$_3$ structure with long and short Mn–O distances in the *ab* plane. We, therefore, repeated the same computational experiment but now with an embedding that only reflects the tilting of the MnO$_6$ octahedra and not the Jahn-Teller distortion. Results are depicted by the curve with the light blue triangles. Although the minimum is less deep and located at smaller Jahn-Teller distortion, we clearly observe a tendency toward Jahn-Teller distortion with this embedding. The fact that all collective effects are missing explains the shallowness of the curve. Finally, we observe a minimum at small distortions for CaFeO$_3$ (green diamonds). This weak tendency to deform the perfect octahedral oxygen coordination of Fe can be ascribed to the appearance of the

Jahn-Teller active NCT determinant in the cluster wave function, cf. Table III. Actually, the experimental x-ray structure reflects a small Jahn-Teller distortion of the FeO$_6$ octahedron.[3] Raman scattering measurements[36] confirm the existence of Jahn-Teller distortions in CaFeO$_3$, which were also explained by the admixture of Fe^{4+}L configurations to the wave function.

VII. CONCLUSIONS

The transformation of the commonly used natural orbitals to optimal atomic orbitals provides us a practical scheme to interpret the CASSCF wave function in terms of valence bond terms as NCT, CT, and DCT configurations. It may be useful to remark that relative small mixing in the natural orbitals lead to rather large CT contributions to the wave function expressed in atomic orbitals. This means that the delocalization tails of the natural orbitals onto neighboring centers are a very efficient way to account for CT, DCT, or even higher excitations. The disadvantage of expressing the wave function with these delocalized orbitals is the difficulty to quantify the relative importance of the different types of excitations.

The ionic model is too simple as a starting point to explain the existence or absence of Jahn-Teller distortions in the here considered perovskites. The high formal charges of the TM ions induce large CT effects such that the CT configuration can become the leading determinant in the wave function expansion.

The embedded cluster model gives of course only a partial view of Jahn-Teller distortions in perovskites. Only local distortions can be addressed and there is no account of the collective nature. The present analysis of the cluster wave function and the dependence of the ground state energy as function of the distortion still gives useful insights in terms of local electronic configurations which can be at the origin of the collective effects.

The present analyses of the wave function, expressed in optimal atomic orbitals, is not limited to solid-state systems in which the ionic model is usually applied. It is also a practical and simple tool to interpret CASSCF wave functions of molecules and covalent solids.

[1] J. Rodríguez-Carvajal, B. Hennion, F. Moussa, H. Moudden, L. Pinsard, and A. Revcolevschi, Phys. Rev. B **57**, 3189 (1998).
[2] E. O. Wollan and W. C. Koehler, Phys. Rev. **100**, 545 (1955).
[3] P. M. Woodward, D. E. Cox, E. Moshopoulou, A. W. Sleight, and S. Moritomo, Phys. Rev. B **62**, 844 (2000).
[4] K. R. Poeppelmeier, M. E. Leonowicz, J. C. Scanlon, J. M. Longo, and W. B. Yelon, J. Solid State Chem. **45**, 71 (1982).
[5] M. A. Buijse and E. J. Baerends, J. Chem. Phys. **93**, 4129 (1990).
[6] K. Pierloot, E. van Praet, L. G. Vanquickenborne, and B. O. Roos, J.

Phys. Chem. **97**, 12220 (1993).

[7] A. Al-Abdalla, L. Seijo, and Z. Barandiarán, J. Chem. Phys. **109**, 6396 (1998).

[8] J.-P. Malrieu, N. Guihéry, C. J. Calzado, and C. Angeli, J. Comput. Chem. **28**, 35 (2007).

[9] Z. Barandiarán and L. Seijo, J. Chem. Phys. **89**, 5739 (1988).

[10] B. O. Roos, P. R. Taylor, and P. E. M. Siegbahn, Chem. Phys. **48**, 157 (1980).

[11] K. Andersson, P.-Å. Malmqvist, B. O. Roos, A. J. Sadlej, and K. Wolinski, J. Phys. Chem. **94**, 5483 (1990).

[12] K. Andersson, P.-Å. Malmqvist, and B. O. Roos, J. Chem. Phys. **96**, 1218 (1992).

[13] T. Thorsteinsson, D. L. Cooper, J. Gerratt, P. B. Karadakov, and M. Raimondi, Theor. Chim. Acta **93**, 343 (1996).

[14] T. Thorsteinsson and D. L. Cooper, Int. J. Quantum Chem. **70**, 637 (1998).

[15] K. Hirao, H. Nakano, K. Nakayma, and M. Dupuis, J. Chem. Phys. **105**, 9227 (1996).

[16] L. Seijo and Z. Barandiarán, J. Chem. Phys. **94**, 8158 (1991).

[17] L. Seijo (unpublished).

[18] C. Sousa, J. Casanovas, J. Rubio, and F. Illas, J. Comput. Chem. **14**, 680 (1993).

[19] R. Pou-Amérigo, M. Merchán, I. Nebot-Gil, P.-O. Widmark, and B. O. Roos, Theor. Chim. Acta **92**, 149 (1995).

[20] P.-O. Widmark, P.-Å. Malmqvist, and B. O. Roos, Theor. Chim. Acta **77**, 291 (1990).

[21] M. A. Nygren, L. G. M. Pettersson, Z. Barandiarán, and L. Seijo, J. Chem. Phys. **100**, 2010 (1994).

[22] T. H. Dunning, Jr., B. H. Botch, and J. F. Harrison, J. Chem. Phys. **72**, 3419 (1980).

[23] C. de Graaf, R. Broer, and W. C. Nieuwpoort, Chem. Phys. **208**, 35 (1996).

[24] G. J. M. Janssen and W. C. Nieuwpoort, Int. J. Quantum Chem., Quantum Chem. Symp. **22**, 679 (1988).

[25] K. Pierloot, E. Tsokos, and L. G. Vanquickenborne, J. Phys. Chem. **100**, 16545 (1996).

[26] K. Pierloot and S. Vancoillie, J. Chem. Phys. **125**, 124303 (2006).

[27] G. Karlström, R. Lindh, P.-Å. Malmqvist *et al.*, Comput. Mater. Sci. **28**, 222 (2003).

[28] J. Casanovas, A. Lorda, C. Sousa, and F. Illas, Int. J. Quantum Chem. **52**, 281 (1994).

[29] A. J. Millis, P. B. Littlewood, and B. I. Shraiman, Phys. Rev. Lett. **74**, 5144 (1995).

[30] J. L. Pascual, L. Seijo, and Z. Barandiarán, Phys. Rev. B **53**, 1138 (1996).

[31] F. García-Fernández, C. Sousa, J. A. Aramburu, M. T. Barriuso, and M. Moreno, Phys. Rev. B **72**, 155107 (2005).

[32] W. E. Pickett and D. J. Singh, Phys. Rev. B **53**, 1146 (1996).

[33] P. Ravindran, A. Kjekshus, H. Fjellvåg, and O. Eriksson, Phys. Rev. B **65**, 064445 (2002).

[34] D. Muñoz, N. M. Harrison, and F. Illas, Phys. Rev. B **69**, 085115 (2004).

[35] J. M. García-Lastra, M. T. Barriuso, J. A. Aramburu, and M. Moreno, Chem. Phys. **317**, 103 (2005).

[36] S. Ghosh, N. Kamaraju, A. Fujimori, Y. Takeda, S. Ishiwata, S. Kawasaki, M. Azuma, M. Takano, and A. K. Sood, Phys. Rev. B **71**, 245110 (2005).